

Accuracy of the Heyd-Scuseria-Ernzerhof hybrid functional to describe many-electron interactions and charge localization in semiconductors

Mauricio A. Flores,^{1,*} Walter Orellana,² and Eduardo Menéndez-Proupin³

¹*Facultad de Ingeniería y Tecnología, Universidad San Sebastián, Bellavista 7, Santiago 8420524, Chile*

²*Departamento de Ciencias Físicas, Universidad Andres Bello, Sazié 2212, Santiago 8370136, Chile*

³*Departamento de Física, Facultad de Ciencias, Universidad de Chile, Las Palmeras 3425, Ñuñoa, Santiago 7800003, Chile*



(Received 8 May 2018; revised manuscript received 18 September 2018; published 17 October 2018)

Hybrid functionals, which mix a fraction of Hartree-Fock exchange with local or semilocal exchange, have become increasingly popular in quantum chemistry and computational materials science. Here, we assess the accuracy of the Heyd-Scuseria-Ernzerhof (HSE) hybrid functional to describe many-electron interactions and charge localization in semiconductors. We perform diffusion quantum Monte Carlo calculations to obtain the accurate ground-state spin densities of the negatively charged $(\text{SiV})^-$ and the neutral $(\text{SiV})^0$ silicon-vacancy center in diamond and of the cubic silicon carbide (3C-SiC) with an extra electron. We compare our diffusion quantum Monte Carlo results with those obtained with the HSE functional and find a good agreement between the two methods for $(\text{SiV})^-$ and $(\text{SiV})^0$, whereas the correct description of 3C-SiC with an extra electron crucially depends on the amount of Hartree-Fock exchange included in the functional. Also, we examine the case of the neutral Cd vacancy in CdTe, for which we assess the performance of HSE versus the many-body *GW* approximation for the description of the position of the defect states in the band gap.

DOI: [10.1103/PhysRevB.98.155131](https://doi.org/10.1103/PhysRevB.98.155131)

I. INTRODUCTION

Density functional theory (DFT) [1,2] has become the leading method for electronic structure calculations in materials science, quantum chemistry, and condensed-matter physics [3,4]. The DFT formalism shows that ground-state properties of a many-electron system can be determined from the knowledge of the electron density distribution alone, thereby avoiding the computation of massively complex many-dimensional wave functions. The ground-state density is described by a single determinant with all many-body effects included in one term, the exchange-correlation functional. Unfortunately, the exact functional is unknown and it is necessary to use practical approximations.

Extensive research efforts have been dedicated to obtain better approximations to the exact exchange-correlation functional. Earlier approximations were the local density approximation (LDA) [5], which considers the exchange and correlation interaction as obtained from a homogeneous electron gas, and the generalized gradient approximation (GGA) [6,7], which adds gradient terms to the LDA approach. Both approximations are computationally efficient and give reasonable results for ground-state properties of molecules and solids, however, they have limitations that hinder their predictive power. They do not properly account for the long-range dispersion forces in van der Waals systems [8,9], underestimate the energy barriers of chemical reactions, give erroneous dissociation energies of diatomic radicals [10], and severely underestimate the band gap in semiconductors and insulators [11]. Better approximations can be achieved by

including additional information with the energy density. In this way, meta-GGAs [12,13] incorporate the second-order gradient of the density, giving accurate results when the system is near mechanical equilibrium but still failing when bonds are stretched, as nonlocality dominates [14]. Hybrid GGAs [15,16] include nonlocality information by mixing a fraction of Hartree-Fock exchange with local or semilocal exchange. They improve the description of the energy band gap in semiconductors and insulators, but the results critically depend on the amount of Hartree-Fock exchange included in the functional. Although some studies have shown that hybrid functionals such as the Heyd-Scuseria-Ernzerhof (HSE) [16,17] yield a good accuracy for defect energy levels in solids [18,19], other calculations have revealed serious discrepancies when they are compared with more accurate methods such as the diffusion quantum Monte Carlo (DMC) [20–22]. More recently, double-hybrid GGAs have been proposed [23–26]. In addition to a fraction of Hartree-Fock exchange, they include a fraction of the second-order Møller-Plesset correlation within the random phase approximation.

Recently, Medvedev and coworkers [27] pointed out that DFT is straying from the path toward the exact functional, which should give “the right answer for the right reason” [28,29]. They show that modern highly parameterized functionals have improved the energies while not always improving the electron densities. Here, we investigate the performance of the HSE hybrid functional to describe many-electron interactions and charge localization in semiconductors beyond that of pristine bulk materials. We present a comparison of electron densities calculated using the increasingly popular HSE functional with those obtained with the accurate wave-function-based DMC method [30–32]. We assess the accuracy of the HSE for the description of defective

*mflores@next-solar.net

diamond and cubic silicon carbide (3C-SiC) with an extra electron. Additionally, we compare the performance of the HSE with the many-body GW approximation [33,34] for the description of the position of localized defect levels introduced in defective CdTe. In the latter case, we find that the two approaches qualitatively differ in determining the position of the antibonding orbital introduced by the neutral Cd vacancy with respect to the conduction band edge, irrespective of the amount of Hartree-Fock exchange included in the hybrid functional.

II. METHODS

Computational details

We performed density functional calculations using the optimized norm-conserving pseudopotential library v0.4 [35] generated by Hamann [36] in a plane-wave basis set with an energy cutoff of 80 Ry. We used the HSE hybrid functional with the standard exchange and screening parameters, as implemented in the QUANTUM ESPRESSO code. [37,38]

Our DMC calculations were performed using the CASINO code [39]. We used trial wave functions (Ψ_T) of the Slater-Jastrow [40,41] type,

$$\Psi_T = \det\{\psi_\uparrow\} \det\{\psi_\downarrow\} e^J, \quad (1)$$

where the determinants are composed of single-particle orbitals obtained from spin-polarized DFT calculations performed using the QUANTUM ESPRESSO code package [37,38]. We used Trail and Needs norm-conserving pseudopotentials [42,43] with a plane-wave energy cutoff of ~ 4081.71 eV ($=150$ Ha). Electron terms, electron-nucleus terms, and electron-electron-nucleus terms were included in the Jastrow correlation factor (e^J), whose parameters were optimized through variance minimization of the local energy at the variational Monte Carlo level [44,45]. This process was followed by DMC calculations within the fixed-node approximation [46–48]. In this approach, the diffusion process is confined inside the connected nodal region of Ψ_T , where the wave function is always positive and vanishes at the boundaries. Unless the nodal surface is exactly correct the fixed-node approximation gives an upper bound to the true ground-state energy. In general, the nodal structures given by PBE or LDA wave functions multiplied by an optimized Jastrow factor to correct for electron correlation are found to be quite accurate for systems without partially occupied d orbitals [49–53].

In our calculations, the trial wave functions were generated from spin-polarized DFT-PBE calculations using 64-atom supercells for diamond and 3C-SiC, at the R point only. At the DMC level, the spin density was calculated using the mixed estimator [30]. We used a DMC time step τ of 0.01 a.u. and a target population of 5048 walkers, which resulted in an acceptance ratio greater than 99.6%. To reduce the bias due to pseudopotential localization, we used the T-move scheme proposed by Casula [54]. Additionally, to establish the difference among the methods under study, we calculated the dissociation curve of H_2 by placing the molecule in a cubic supercell of side 18 Å.

For the Cd vacancy in CdTe, we performed many-body G_0W_0 calculations using the ABINIT simulation code [55,56]. The calculations were performed in 64-atom supercells, using

a $2 \times 2 \times 2$ \mathbf{k} -point mesh to obtain a converged DFT charge density that was then used as a starting point for a subsequent COHSEX (Coulomb-hole screened exchange) + G_0W_0 calculation at the Γ point only. We employed projector-augmented wave [57] pseudopotentials from the GBRV library [58] and a plane-wave energy cutoff of 30 Ry. In addition, we used a 20-Ry energy cutoff to represent the dielectric matrix and 3200 bands plus the extrapolation of Bruneval and Gonze [59]. The frequency dependence of the dielectric matrix was approximated by the plasmon-pole model of Hybertsen and Louie [60].

III. RESULTS AND DISCUSSION

A. Many-electron interactions in the silicon-vacancy center in diamond

Defects in diamond have been proposed as promising candidates to realize single-photon sources with applications in quantum cryptography [61], magnetic field sensing [62,63], and quantum optics [64–66]. In particular, the negatively charged silicon-vacancy center (SiV^-) [67–72] has attracted considerable interest due to its exceptional optical properties. The (SiV^-) has a split-vacancy configuration wherein the Si atom adopts a position equidistant from two carbon vacancies. This configuration has D_{3d} symmetry and six carbon dangling bonds, which combine into a_{1g} , a_{2u} , e_u , and e_g defect orbitals. Eleven electrons fill these orbitals: six electrons are provided by the dangling bonds, four sp^3 electrons are donated by the Si impurity, and one additional electron is captured by the defect center, leading to the $a_{1g}^2 a_{2u}^2 e_u^4 e_g^3$ open-shell electronic configuration. As the e_g state is partially filled, the (SiV^-) should, in principle, undergo a Jahn-Teller distortion to a lower symmetry point group. However, photoluminescent emission and excitation experiments [73] as well as Zeeman studies [74] suggest that this defect center retains the D_{3d} symmetry. The origin remains unclear, but an explanation is given in terms of a dynamic Jahn-Teller effect [73,75–78].

One way to assess the accuracy of the hybrid functional for the description of many-electron interactions is by first computing the spin density at the HSE level and then comparing the results with those obtained using the more accurate quantum Monte Carlo method. In the latter case, the dependence of the many-electron wave function on electron-electron separations is first taken into account at the variational Monte Carlo level by including an optimized Jastrow correlation factor [44]. Additionally, the projection operation in the subsequent DMC calculation includes all dynamic correlations (whether or not included in the optimized trial function) for states that fall within the space consistent with the fixed node constraint.

We first investigate the (SiV^-) in the symmetrical D_{3d} configuration, which has orbital and spin degeneracy, and in the C_{2h} configuration, where the e_g states are split by a static Jahn-Teller distortion [79]. In the former case, there are three electrons in the e_g level, leaving a single hole with e symmetry and a many-body state with 2E total spin symmetry. Schematics of the electronic structure of the D_{3d} configuration, based on a simple molecular orbital model, and the spin density obtained by HSE and DMC calculations are

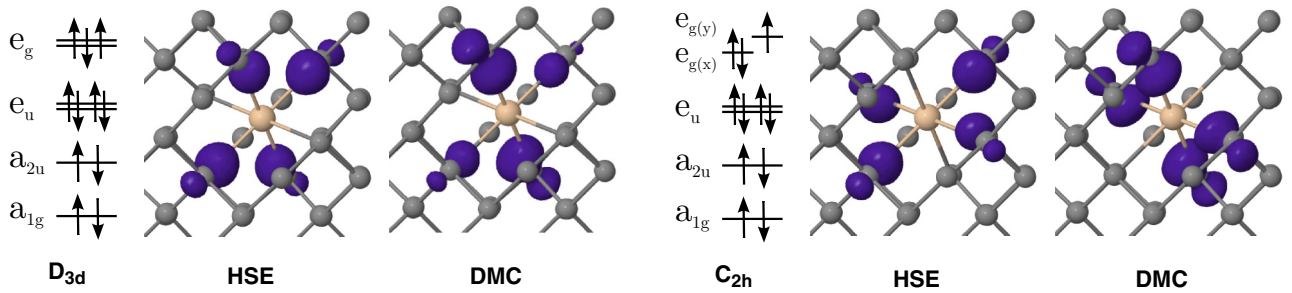


FIG. 1. Schematic of the electronic structure and the corresponding electron spin density ($\rho = 20\%$ of the maximum) obtained by HSE and DMC calculations of the negatively charged silicon-vacancy center in diamond in D_{3d} (left) and C_{2h} symmetry (right).

shown in Fig. 1 (left). Both methods give qualitatively the same results [80]. In the case of the HSE, the inclusion of a fraction of nonlocal exact exchange breaks the symmetry of the system, lifting the degeneracy of the partially occupied e_g level in the spin-down channel. Moreover, if the system is allowed to relax, it finds its minimum in C_{2h} symmetry. In the DMC, inclusion of the spatially dependent correlation energy (i.e., electron-electron interactions beyond their mean-field average) breaks the spin degeneracy of the single-particle e_g states. As the resulting spin density is inconsistent with the symmetry mandated by the D_{3d} point group, a structural distortion to a lower symmetry group is suggested.

According to the Jahn-Teller theorem [81], the orbital degeneracy of the partially occupied e_g level can be lifted by a small structural distortion to a less symmetric point group. We found two configurations with C_{2h} symmetry where two carbon dangling bonds are located ~ 0.03 Å closer to and ~ 0.03 Å farther from the silicon impurity. At the DMC level, the former configuration is more stable by about 0.12 eV. Figure 1 (right) shows schematics of the electronic structure of this configuration and the corresponding spin density obtained by HSE and DMC calculations. The HSE result shows that the spin density is localized equally on the four C atoms located farther away from the Si atom. On the other hand, the DMC indicates that the spin density is localized on the two C atoms located closer to the Si atom and on two of the four C atoms located farther from the impurity [82]. Nevertheless, the HSE functional can correctly describe the localization of a hole on the $e_{g(y)}$ state. It is worth mentioning the recent work of Bockstedte *et al.* [83], which highlights the importance of dynamic correlation effects on the energy-level structure of the excited state of the nitrogen-vacancy center in diamond.

It is also suitable to investigate the silicon vacancy in the neutral charge state (SiV^0). This complex has an $a_{1g}^2 a_{2u}^2 e_u^4 e_g^2$ electronic configuration, which, according to Hund's rule, results in an $S = 1$ ground-state electron spin configuration [84]. Schematics of the electronic structure as well as a comparison of the spin densities obtained by HSE vs DMC calculations are shown in Fig. 2. In contrast to $(\text{SiV})^-$, we observe a qualitative agreement between the HSE and the DMC. Although the HSE spin density is slightly overlocalized compared with the DMC result, in both cases the distribution has its maxima equally centered on the six carbon dangling bonds.

Next, we discuss how many-electron interactions are treated in the Kohn-Sham density functional theory and within

the DMC approximation. In the case of electrons with parallel spins, the antisymmetry requirement of the wave function fulfills the Pauli exclusion principle and keeps electrons apart, introducing a so-called Fermi hole [85]. However, the Pauli exclusion principle exerts only a small influence on electrons of opposite spin and thus Coulomb interactions should be explicitly taken into account. Therefore, we should note that correlation errors mainly affect the description of electrons having opposite spins. In DFT, electron interactions are approximated by a mean-field potential and the many-body wave function is represented by a single Slater determinant composed of single-particle orbitals. This is a good approximation for systems of slowly varying density, but it is insufficient for situations of degeneracy or near degeneracy [86–88] or when electron correlations depend on the shape of the ground-state vacant orbitals or excited-state orbitals. In these cases, the system is poorly described by a single Slater determinant. On the other hand, in the DMC the effect of short-range correlations is accounted for by a Jastrow correlation factor, which reduces the amplitude of the wave function when electrons are close to each other, thereby making the wave function explicitly dependent on the position.

The difference between the two approximations can be clearly seen by considering the stretched H_2 molecule, the simplest case of a strongly correlated system, where the true (interacting) ground state is a singlet [89]. The ground-state energy of the hydrogen molecule was previously calculated by Traynor *et al.* [90] using the quantum Monte Carlo method. Our results for the dissociation curve of the H_2

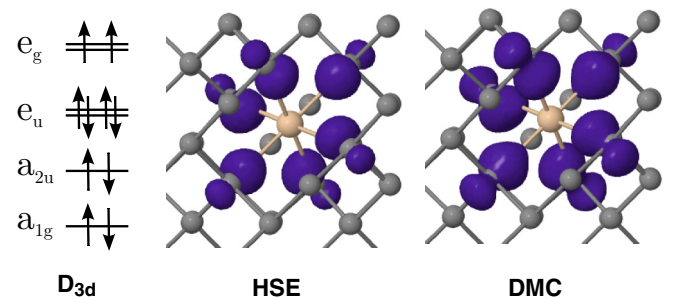


FIG. 2. Schematic of the electronic structure and the corresponding electron spin density ($\rho = 20\%$ of the maximum) obtained by HSE and DMC calculations of the silicon-vacancy center in diamond in the neutral charge state in D_{3d} symmetry.

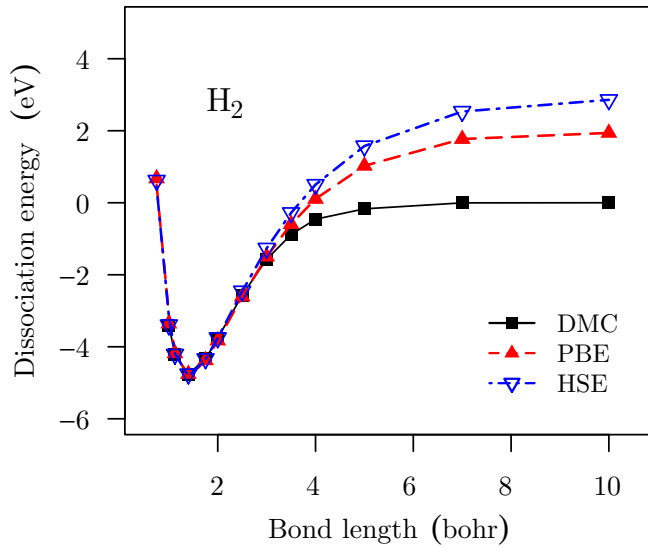


FIG. 3. Dissociation energy curve of the H_2 molecule obtained by DMC, PBE, and HSE calculations.

molecule obtained within the DFT approximation (employing both PBE and HSE exchange-correlation functionals) and with the DMC method are shown in Fig. 3. According to the mean-field approximation of DFT, the probability of finding both electrons in the same atom is always $1/2$, regardless of the bond length [91]. This is a good approximation when the atoms are near their equilibrium bond length (~ 1.4 bohr), but it fails in the dissociation limit, where each H atom has a half spin-up electron and a half spin-down electron [88].

The reason behind the good accuracy of the HSE in the description of $(SiV)^0$ might be explained by the fact that in this case there are two electrons with parallel spins occupying the e_g orbital. Moreover, it was demonstrated that this many-body state can always be represented by a single Slater determinant [92]. In contrast, the $(SiV)^-$ center has two electrons of opposite spins occupying the e_g orbital, thus electron-electron interactions beyond their mean-field average may become important.

B. Small polarons in 3C-SiC

It was recently pointed out that the inclusion of a fraction of the Hartree-Fock interaction in hybrid functionals may introduce a spurious exchange splitting between occupied and unoccupied states [93–95]. In spin-polarized calculations, this effect could lead to unusually large magnetic moments [93], wrong magnetic ground states [96], and a slow convergence of the total energy of the system with respect to the supercell size [97,98].

In the following, we investigate the effects of the inclusion of the Hartree-Fock interaction in the HSE functional by considering the negatively charged 3C-SiC. The excess electron may (i) self-localize by coupling to a lattice distortion, forming a polaron, or (ii) retain its free-carrier character. For TiO_2 , it was found that the solution crucially depends on the fraction of the Hartree-Fock exchange included in the exchange-correlation functional [99,100].

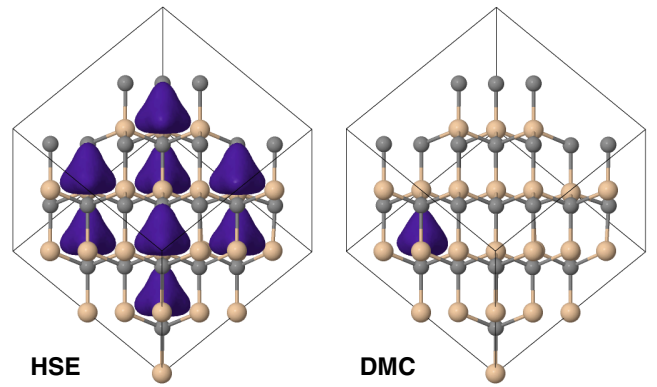


FIG. 4. Electron spin density ($\rho = 40\%$ of the maximum) of 3C-SiC obtained by HSE (left) and DMC (right) calculations. Beige and turquoise spheres represent Si and C atoms, respectively.

We performed spin-polarized calculations to determine the ground state of the negatively charged 3C-SiC system. We added an extra electron to the conduction band and then allowed the system to relax. Our calculations were performed in a 64-atom supercell, using the HSE functional ($\alpha = 25\%$) for structural relaxations. We found a slightly distorted structure in which one C-Si bond is stretched by ~ 0.07 Å [101]. In Fig. 4, we compare the spin density obtained by HSE and DMC calculations. We observe that both approximations give qualitatively different results. According to the HSE, the negatively charged 3C-SiC is an electridelike compound [102–104] which is characterized by charge localization in interstitial regions; on the other hand, the DMC predicts the formation of a small polaron. The HSE wave function has large magnetic moments on the Si atoms near the local maxima of the spin density and exhibits negative values on the nearby C atoms. We found that the unusual HSE result is due to a finite size effect, a direct consequence of the long-range nature of the Hartree-Fock exchange that converges extremely slowly with respect to the supercell size. The same result as shown in Fig. 4 is obtained using a $2 \times 2 \times 2$ k -point mesh displaced from the Γ point, which is equivalent to a single k -point calculation in a 512-atom supercell. However, if we decrease the fraction of the Hartree-Fock exchange to 10% or use a finer k -point mesh, we find that the spin density is in close agreement with the DMC result. The form of the long-range tail of the Coulomb interaction critically depends on the screening parameter (μ), which defines the extent of the Hartree-Fock exchange in real space [105]. Therefore, we strongly recommend the use of large simulation cells and the careful choice of the amount of Hartree-Fock exchange included in the hybrid functional.

C. Localized defect levels in the band gap

In the simulation of point defects in semiconductors and insulators, a correct description of the band gap as well as the absolute position of the band edges is of critical importance [106,107]. The severe underestimation of the band gap in standard DFT has led to large discrepancies and conflicting results among theoretical calculations. Hybrid functionals can give reliable band gaps for most semiconductors

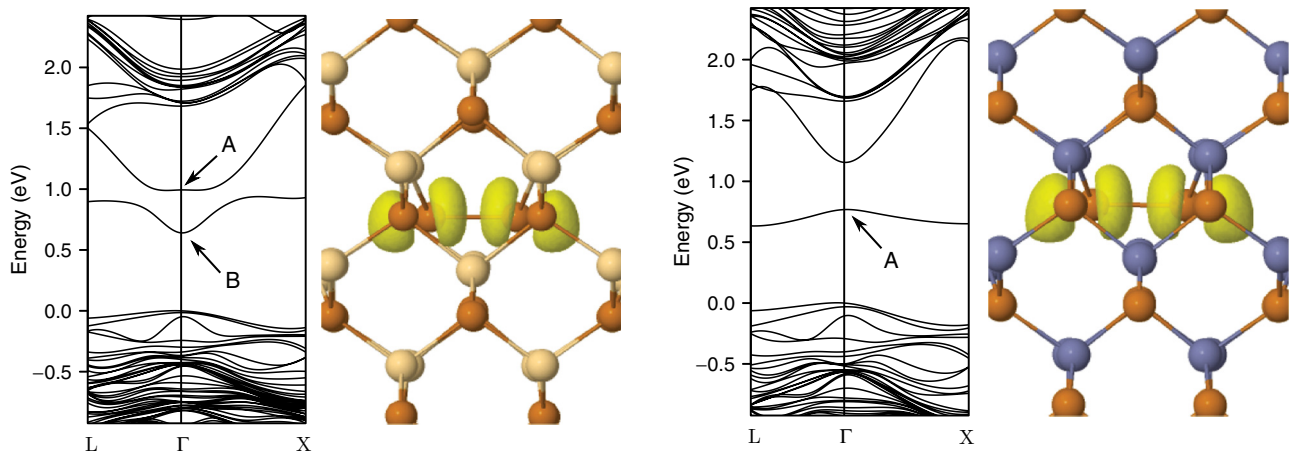


FIG. 5. Electronic band structures and charge density isosurfaces ($\rho = 0.002e/\text{bohr}^3$) corresponding to the energy level labeled A of the neutral cation vacancy in CdTe (left) and ZnTe (right), in C_{2v} symmetry. Brown spheres represent Te atoms; beige and azure spheres represent Cd and Zn atoms, respectively. Calculations were performed at the DFT-PBE level in a 128-atom supercell.

when an optimum system-dependent fraction of Hartree-Fock exchange energy is used [108]. Moreover, it is commonly assumed that they can give a reliable description of defect states [19,22,108], although the use of the same parameters to describe orbitals with distinct degrees of localization seems questionable. In the following, we assess the accuracy of the HSE functional in the not uncommon case when a localized defect state merges with one of the band edges of the host. We consider the Cd vacancy in CdTe, which is among the most important native defects in this semiconductor.

The Cd vacancy in CdTe has been extensively investigated both theoretically and experimentally [109,110]; still, several aspects remain unclear. In the neutral charge state, the Cd vacancy undergoes a structural distortion from T_d to C_{2v} symmetry. The situation is similar to the well-known AX distortion [98,111], where two Te atoms move toward each other to form a new bond. The net result is the loss of one bond (as each Te atom breaks one bond with a Cd atom) and the creation of an empty antibonding orbital. At the DFT-PBE level, this antibonding state is strongly hybridized with the conduction-band minimum (CBM), as shown in Fig. 5 (left). However, this effect is likely to be an artifact of DFT due to the fact that the CdTe band gap is too small such that the antibonding level erroneously lies above the CBM at the Γ point. This can be seen by considering the isoelectronic case of the neutral Zn vacancy in ZnTe, where the antibonding state appears well isolated in the band gap.

In Fig. 5, we compare the DFT-PBE band structure and the squared wave function corresponding to the antibonding level (labeled A) of the neutral cation vacancy in CdTe and ZnTe. In contrast to CdTe, in the case of ZnTe the unoccupied antibonding level lies isolated in the band gap of the host, as the CBM is higher in energy. To accurately obtain the position of this antibonding level introduced by the Cd vacancy in CdTe, we performed many-body GW calculations that can give accurate band structures of solids [112–114]. We used DFT-PBE wave functions as a starting point for a subsequent COHSEX + G_0W_0 perturbative calculation. We found that the unoccupied antibonding state lies 0.26 eV below the CBM.

Taking the G_0W_0 result as a reference, a natural question arises: Is the HSE hybrid functional able to correctly describe the position of the antibonding orbital associated with the neutral Cd vacancy in CdTe? We performed HSE calculations using 128- and 250-atom supercells in which the Brillouin zone was sampled at the Γ point only. These calculations were performed using projector-augmented wave potentials, as implemented in the Vienna *ab initio* simulation package [115]. We found that the HSE gives a band gap of 1.41 eV, in good agreement with the COHSEX + G_0W_0 result of 1.42 eV. However, the HSE retains the PBE result by placing the antibonding orbital 0.48 eV above the CBM. A similar behavior was previously reported for ZnO:Co [116,117], where DFT results are incorrect for the optical absorption and the Co $d-d$ splitting is overestimated by of the order of 300% when the fraction of Hartree-Fock exchange corresponds to the one necessary to reproduce the experimental band gap of ZnO [116]. Another example is the carbon vacancy in 3C-SiC, where the position of the localized defect state erroneously appears above the CBM [118].

The failure of the HSE to describe the position of the antibonding orbital in the neutral Cd vacancy in CdTe is an example of the drawback of the uniform treatment of electronic states with distinct degrees of localization. This issue may be corrected through the addition of empirical nonlocal external potentials [119], by using local hybrid functionals that use a position-dependent mixture of local and exact exchange [120,121] or the orbital-dependent exact exchange extension of hybrid functionals proposed by Ivády *et al.* [122,123]. The latter approach has the advantage that the orbital-dependent parameter can be obtained self-consistently based on the analogy of quasiparticle equations and hybrid-DFT single-particle equations [123]. A recommendation to practitioners studying defects in semiconductors or any system having states with different degrees of localization is always to plot the band structure of the system (at least using computationally efficient local or semilocal functionals) to identify problems analogous to the one presented in this section. In these cases the use of more advanced methods such as the G_0W_0 is highly recommended.

IV. SUMMARY

We have investigated the accuracy of the HSE hybrid exchange-correlation functional in the description of three systems with different levels of complexity: the negatively charged and the neutral silicon-vacancy center in diamond, pristine 3C-SiC with an extra electron, and the neutral Cd vacancy in CdTe.

Our results show that the HSE functional can accurately describe many-electron interactions in systems with moderate correlations, such as the neutral and the negatively charged silicon-vacancy center in diamond. Moreover, the application of the HSE functional to systems with different degrees of localization shows systematic errors: (i) Due to the slow convergence of the Hartree-Fock exchange with respect to the supercell size, it may predict an incorrect ground state for

negatively charged 3C-SiC; and (ii) when localized defect states artificially merge with delocalized (Bloch-like) conduction-band states at the DFT-PBE level, as in the case of the neutral Cd vacancy in CdTe, the HSE corrects the band gap but retains the spurious hybridization given by the PBE, predicting an incorrect position of the localized level with respect to the CBM.

ACKNOWLEDGMENTS

This paper was supported by the Fondo Nacional de Desarrollo Científico y Tecnológico (FONDECYT, Chile) under Grants No. 1170480 (W.O.) and No. 1171807 (M.A.F. and E.M-P.). Powered@NLHPC: This research was partially supported by the supercomputing infrastructure of the NLHPC (ECM-02).

-
- [1] P. Hohenberg and W. Kohn, *Phys. Rev.* **136**, B864 (1964).
 [2] W. Kohn, *Rev. Mod. Phys.* **71**, 1253 (1999).
 [3] P. J. Hasnip, K. Refson, M. I. Probert, J. R. Yates, S. J. Clark, and C. J. Pickard, *Phil. Trans. R. Soc. A* **372**, 20130270 (2014).
 [4] R. O. Jones, *Rev. Mod. Phys.* **87**, 897 (2015).
 [5] W. Kohn and L. J. Sham, *Phys. Rev.* **140**, A1133 (1965).
 [6] A. D. Becke, *Phys. Rev. A* **38**, 3098 (1988).
 [7] J. P. Perdew, K. Burke, and M. Ernzerhof, *Phys. Rev. Lett.* **77**, 3865 (1996).
 [8] R. Jones, *J. Chem. Phys.* **71**, 1300 (1979).
 [9] W. Kohn, Y. Meir, and D. E. Makarov, *Phys. Rev. Lett.* **80**, 4153 (1998).
 [10] P. Mori-Sánchez, A. J. Cohen, and W. Yang, *J. Chem. Phys.* **125**, 201102 (2006).
 [11] J. P. Perdew and M. Levy, *Phys. Rev. Lett.* **51**, 1884 (1983).
 [12] A. D. Becke, *J. Chem. Phys.* **109**, 2092 (1998).
 [13] J. Tao, J. P. Perdew, V. N. Staroverov, and G. E. Scuseria, *Phys. Rev. Lett.* **91**, 146401 (2003).
 [14] J. P. Perdew, V. N. Staroverov, J. Tao, and G. E. Scuseria, *Phys. Rev. A* **78**, 052513 (2008).
 [15] J. Jaramillo, G. E. Scuseria, and M. Ernzerhof, *J. Chem. Phys.* **118**, 1068 (2003).
 [16] J. Heyd, G. E. Scuseria, and M. Ernzerhof, *J. Chem. Phys.* **118**, 8207 (2003).
 [17] J. Heyd, G. E. Scuseria, and M. Ernzerhof, *J. Chem. Phys.* **124**, 219906 (2006).
 [18] D. K. Lewis, M. Matsubara, E. Bellotti, and S. Sharifzadeh, *Phys. Rev. B* **96**, 235203 (2017).
 [19] W. Chen and A. Pasquarello, *Phys. Rev. B* **96**, 020101 (2017).
 [20] J. A. Santana, J. T. Krogel, J. Kim, P. R. Kent, and F. A. Reboredo, *J. Chem. Phys.* **142**, 164705 (2015).
 [21] J. A. Santana, J. T. Krogel, P. R. Kent, and F. A. Reboredo, *J. Chem. Phys.* **147**, 034701 (2017).
 [22] M. Gerosa, C. Bottani, C. Di Valentin, G. Onida, and G. Pacchioni, *J. Phys. Condens. Matter* **30**, 044003 (2017).
 [23] S. Grimme, *J. Chem. Phys.* **124**, 034108 (2006).
 [24] K. Sharkas, J. Toulouse, and A. Savin, *J. Chem. Phys.* **134**, 064113 (2011).
 [25] N. Q. Su, Z. Zhu, and X. Xu, *Proc. Natl. Acad. Sci. U.S.A.* **115**, 2287 (2018).
 [26] Z.-H. Cui, Y.-C. Wang, M.-Y. Zhang, X. Xu, and H. Jiang, *J. Phys. Chem. Lett.* **9**, 2338 (2018).
 [27] M. G. Medvedev, I. S. Bushmarinov, J. Sun, J. P. Perdew, and K. A. Lyssenko, *Science* **355**, 49 (2017).
 [28] M. Korth, *Angew. Chem. Int. Ed* **56**, 5396 (2017).
 [29] S. Hammes-Schiffer, *Science* **355**, 28 (2017).
 [30] W. M. C. Foulkes, L. Mitas, R. J. Needs, and G. Rajagopal, *Rev. Mod. Phys.* **73**, 33 (2001).
 [31] B. M. Austin, D. Y. Zubarev, and W. A. Lester, *Chem. Rev.* **112**, 263 (2012).
 [32] M. Dubecký, L. Mitas, and P. Jurečka, *Chem. Rev.* **116**, 5188 (2016).
 [33] L. Hedin, *Phys. Rev.* **139**, A796 (1965).
 [34] M. S. Hybertsen and S. G. Louie, *Phys. Rev. Lett.* **55**, 1418 (1985).
 [35] M. Van Setten, M. Giantomassi, E. Bousquet, M. J. Verstraete, D. R. Hamann, X. Gonze, and G.-M. Rignanese, *Comput. Phys. Commun.* **226**, 39 (2018).
 [36] D. R. Hamann, *Phys. Rev. B* **88**, 085117 (2013).
 [37] P. Giannozzi, S. Baroni, N. Bonini, M. Calandra, R. Car, C. Cavazzoni, D. Ceresoli, G. L. Chiarotti, M. Cococcioni, I. Dabo *et al.*, *J. Phys. Condens. Matter* **21**, 395502 (2009).
 [38] P. Giannozzi, O. Andreussi, T. Brumme, O. Bunau, M. B. Nardelli, M. Calandra, R. Car, C. Cavazzoni, D. Ceresoli, M. Cococcioni *et al.*, *J. Phys. Condens. Matter* **29**, 465901 (2017).
 [39] R. Needs, M. Towler, N. Drummond, and P. L. Ríos, *J. Phys.: Condens. Matter* **22**, 023201 (2009).
 [40] J. C. Slater, *Phys. Rev.* **34**, 1293 (1929).
 [41] R. Jastrow, *Phys. Rev.* **98**, 1479 (1955).
 [42] J. Trail and R. Needs, *J. Chem. Phys.* **122**, 014112 (2005).
 [43] J. Trail and R. Needs, *J. Chem. Phys.* **122**, 174109 (2005).
 [44] N. D. Drummond, M. D. Towler, and R. J. Needs, *Phys. Rev. B* **70**, 235119 (2004).
 [45] N. D. Drummond, R. J. Needs, A. Sorouri, and W. M. C. Foulkes, *Phys. Rev. B* **78**, 125106 (2008).
 [46] J. B. Anderson, *J. Chem. Phys.* **63**, 1499 (1975).
 [47] D. M. Ceperley and B. J. Alder, *Phys. Rev. Lett.* **45**, 566 (1980).
 [48] P. J. Reynolds, D. M. Ceperley, B. J. Alder, and W. A. Lester Jr., *J. Chem. Phys.* **77**, 5593 (1982).

- [49] W.-K. Leung, R. J. Needs, G. Rajagopal, S. Itoh, and S. Ihara, *Phys. Rev. Lett.* **83**, 2351 (1999).
- [50] R. Q. Hood, P. R. C. Kent, R. J. Needs, and P. R. Briddon, *Phys. Rev. Lett.* **91**, 076403 (2003).
- [51] D. Alfè and M. J. Gillan, *Phys. Rev. B* **71**, 220101 (2005).
- [52] R. Q. Hood, P. R. C. Kent, and F. A. Reboredo, *Phys. Rev. B* **85**, 134109 (2012).
- [53] J. Kolorenč, S. Hu, and L. Mitas, *Phys. Rev. B* **82**, 115108 (2010).
- [54] M. Casula, *Phys. Rev. B* **74**, 161102 (2006).
- [55] X. Gonze, B. Amadon, P.-M. Anglade, J.-M. Beuken, F. Bottin, P. Boulanger, F. Bruneval, D. Caliste, R. Caracas, M. Côté *et al.*, *Comput. Phys. Commun.* **180**, 2582 (2009).
- [56] X. Gonze, F. Jollet, F. A. Araujo, D. Adams, B. Amadon, T. Applencourt, C. Audouze, J.-M. Beuken, J. Bieder, A. Bokhanchuk *et al.*, *Comput. Phys. Commun.* **205**, 106 (2016).
- [57] P. E. Blöchl, *Phys. Rev. B* **50**, 17953 (1994).
- [58] K. F. Garrity, J. W. Bennett, K. M. Rabe, and D. Vanderbilt, *Comput. Mater. Sci.* **81**, 446 (2014).
- [59] F. Bruneval and X. Gonze, *Phys. Rev. B* **78**, 085125 (2008).
- [60] M. S. Hybertsen and S. G. Louie, *Phys. Rev. B* **34**, 5390 (1986).
- [61] N. Gisin, G. Ribordy, W. Tittel, and H. Zbinden, *Rev. Mod. Phys.* **74**, 145 (2002).
- [62] G. Balasubramanian, P. Neumann, D. Twitchen, M. Markham, R. Kolesov, N. Mizuochi, J. Isoya, J. Achard, J. Beck, J. Tissler *et al.*, *Nat. Mater.* **8**, 383 (2009).
- [63] G. Thiering and A. Gali, *Phys. Rev. B* **96**, 081115 (2017).
- [64] E. Togan, Y. Chu, A. Trifonov, L. Jiang, J. Maze, L. Childress, M. G. Dutt, A. S. Sørensen, P. Hemmer, A. S. Zibrov *et al.*, *Nature* **466**, 730 (2010).
- [65] I. Aharonovich, A. D. Greentree, and S. Praver, *Nat. Photon.* **5**, 397 (2011).
- [66] G. Thiering and A. Gali, *Phys. Rev. B* **98**, 085207 (2018).
- [67] T. Müller, C. Hepp, B. Pingault, E. Neu, S. Gsell, M. Schreck, H. Sternschulte, D. Steinmüller-Nethl, C. Becher, and M. Atatüre, *Nat. Commun.* **5**, 3328 (2014).
- [68] J. N. Becker, J. Görlitz, C. Arend, M. Markham, and C. Becher, *Nat. Commun.* **7**, 13512 (2016).
- [69] J. N. Becker and C. Becher, *Phys. Status Solidi A* **214**, 1700586 (2017).
- [70] S. Häußler, G. Thiering, A. Dietrich, N. Waasem, T. Teraji, J. Isoya, T. Iwasaki, M. Hatano, F. Jelezko, A. Gali *et al.*, *New J. Phys.* **19**, 063036 (2017).
- [71] S. Dhomkar, P. R. Zangara, J. Henshaw, and C. A. Meriles, *Phys. Rev. Lett.* **120**, 117401 (2018).
- [72] E. A. Ekimov, P. S. Sherin, V. S. Krivobok, S. G. Lyapin, V. A. Gavva, and M. V. Kondrin, *Phys. Rev. B* **97**, 045206 (2018).
- [73] L. J. Rogers, K. D. Jahnke, M. W. Doherty, A. Dietrich, L. P. McGuinness, C. Müller, T. Teraji, H. Sumiya, J. Isoya, N. B. Manson *et al.*, *Phys. Rev. B* **89**, 235101 (2014).
- [74] C. Hepp, T. Müller, V. Waselowski, J. N. Becker, B. Pingault, H. Sternschulte, D. Steinmüller-Nethl, A. Gali, J. R. Maze, M. Atatüre *et al.*, *Phys. Rev. Lett.* **112**, 036405 (2014).
- [75] F. S. Ham, *Phys. Rev.* **138**, A1727 (1965).
- [76] A. Gali and J. R. Maze, *Phys. Rev. B* **88**, 235205 (2013).
- [77] G. Thiering and A. Gali, *Phys. Rev. X* **8**, 021063 (2018).
- [78] E. Londero, G. Thiering, L. Razinkovas, A. Gali, and A. Alkauskas, *Phys. Rev. B* **98**, 035306 (2018).
- [79] U. Öpik and M. H. L. Pryce, *Proc. R. Soc. Lond. A* **238**, 425 (1957).
- [80] The HSE spin density was obtained by starting the calculation from an asymmetric initial magnetization. A totally symmetric solution (similar to that depicted in Fig. 2) can be found if the calculation starts from zero magnetization. In the Vienna *ab initio* simulation package code, the symmetric solution can be obtained by specifying $\sigma = 0.2$ (the default value), whereas the asymmetric solution can be found by setting $\sigma = 0.2$. If the PBE functional is used, the spin density is totally symmetric, similar to that depicted in Fig. 2.
- [81] H. A. Jahn and E. Teller, *Proc. R. Soc. Lond. A* **161**, 220 (1937).
- [82] The spin densities are available in Gaussian.cube format at <http://doi.org/10.17632/jyzzjrwhsp.1>.
- [83] M. Bockstedte, F. Schütz, T. Garratt, V. Ivády, and A. Gali, *npj Quantum Mater.* **3**, 31 (2018).
- [84] B. L. Green, S. Mottishaw, B. G. Breeze, A. M. Edmonds, U. F. S. D’Haenens-Johansson, M. W. Doherty, S. D. Williams, D. J. Twitchen, and M. E. Newton, *Phys. Rev. Lett.* **119**, 096402 (2017).
- [85] E. Giner, L. Tenti, C. Angeli, and J.-P. Malrieu, *J. Chem. Phys.* **145**, 124114 (2016).
- [86] A. D. Becke, *J. Chem. Phys.* **119**, 2972 (2003).
- [87] A. J. Cohen, P. Mori-Sánchez, and W. Yang, *J. Chem. Phys.* **129**, 121104 (2008).
- [88] A. J. Cohen, P. Mori-Sánchez, and W. Yang, *Science* **321**, 792 (2008).
- [89] W. Kolos and C. Roothaan, *Rev. Mod. Phys.* **32**, 219 (1960).
- [90] C. A. Traynor, J. B. Anderson, and B. M. Boghosian, *J. Chem. Phys.* **94**, 3657 (1991).
- [91] T. Olsen and K. S. Thygesen, *J. Chem. Phys.* **140**, 164116 (2014).
- [92] P.-O. Löwdin, in *Advances in Chemical Physics*, edited by I. Prigogine (Interscience, London, 1959), Vol. 2, pp. 209–322.
- [93] Y.-R. Jang and B. Deok Yu, *J. Phys. Soc. Jpn.* **81**, 114715 (2012).
- [94] J. Bang, Y. Y. Sun, T. A. Abtew, A. Samanta, P. Zhang, and S. B. Zhang, *Phys. Rev. B* **88**, 035134 (2013).
- [95] W. Gao, T. A. Abtew, T. Cai, Y.-Y. Sun, S. Zhang, and P. Zhang, *Solid State Commun.* **234**, 10 (2016).
- [96] R. Grau-Crespo, H. Wang, and U. Schwingenschlögl, *Phys. Rev. B* **86**, 081101 (2012).
- [97] P. Broqvist, A. Alkauskas, and A. Pasquarello, *Phys. Rev. B* **80**, 085114 (2009).
- [98] M. A. Flores, W. Orellana, and E. Menéndez-Proupin, *Phys. Rev. B* **96**, 134115 (2017).
- [99] A. Janotti, C. Franchini, J. Varley, G. Kresse, and C. Van de Walle, *Phys. Status Solidi RRL* **7**, 199 (2013).
- [100] A. R. Elmaslmane, M. B. Watkins, and K. P. McKenna, *J. Chem. Theory Comput.* **14**, 3740 (2018).
- [101] See Supplemental Material at <http://link.aps.org/supplemental/10.1103/PhysRevB.98.155131> for the distorted 3C-SiC structure.
- [102] J. L. Dye, *Acc. Chem. Res.* **42**, 1564 (2009).
- [103] X. Dong, A. R. Oganov, A. F. Goncharov, E. Stavrou, S. Lobanov, G. Saleh, G.-R. Qian, Q. Zhu, C. Gatti, V. L. Deringer *et al.*, *Nat. Chem.* **9**, 440 (2017).

- [104] M. A. Flores and G. Gutiérrez, [arXiv:1802.08985](#).
- [105] J. H. Skone, M. Govoni, and G. Galli, *Phys. Rev. B* **89**, 195112 (2014).
- [106] M.-H. Du, *J. Phys. Chem. Lett.* **6**, 1461 (2015).
- [107] M. A. Flores, W. Orellana, and E. Menéndez-Proupin, *Comput. Mater. Sci.* **125**, 176 (2016).
- [108] J. Heyd, J. E. Peralta, G. E. Scuseria, and R. L. Martin, *J. Chem. Phys.* **123**, 174101 (2005).
- [109] P. Emanuelsson, P. Omling, B. K. Meyer, M. Wienecke, and M. Schenk, *Phys. Rev. B* **47**, 15578 (1993).
- [110] A. Shepidchenko, B. Sanyal, M. Klintonberg, and S. Mirbt, *Sci. Rep.* **5**, 14509 (2015).
- [111] K. Biswas and M.-H. Du, *Appl. Phys. Lett.* **98**, 181913 (2011).
- [112] M. A. Flores, *Semicond. Sci. Technol.* **33**, 015004 (2018).
- [113] M. A. Flores, E. Menéndez-Proupin, W. Orellana, and J. L. Peña, *J. Phys. D: Appl. Phys.* **50**, 035501 (2017).
- [114] J. Klimeš, M. Kaltak, and G. Kresse, *Phys. Rev. B* **90**, 075125 (2014).
- [115] G. Kresse and J. Furthmüller, *Phys. Rev. B* **54**, 11169 (1996).
- [116] A. Walsh, J. L. F. Da Silva, and S.-H. Wei, *Phys. Rev. Lett.* **100**, 256401 (2008).
- [117] Y. Su, Q. Zhang, N. Zhou, C. Ma, X. Liu, and J. Zhao, *Solid State Commun.* **250**, 123 (2017).
- [118] F. Bruneval, *Nucl. Instr. Methods Phys. Res. B* **277**, 77 (2012).
- [119] S. Lany, H. Raebiger, and A. Zunger, *Phys. Rev. B* **77**, 241201 (2008).
- [120] A. V. Krukau, G. E. Scuseria, J. P. Perdew, and A. Savin, *J. Chem. Phys.* **129**, 124103 (2008).
- [121] A. V. Arbuznikov, H. Bahmann, and M. Kaupp, *J. Phys. Chem. A* **113**, 11898 (2009).
- [122] V. Ivády, R. Armiento, K. Szász, E. Jánzén, A. Gali, and I. A. Abrikosov, *Phys. Rev. B* **90**, 035146 (2014).
- [123] V. Ivády, A. Gali, and I. A. Abrikosov, *J. Phys.: Condens. Matter* **29**, 454002 (2017).